Adjustable Additive Wavelet Transform and Smoothing Filter-Based Intensity Modulation Technique for IKONOS/QuickBird Image Fusion

Te-Ming Tu, Wen-Chun Cheng, Chien-Ping Chang, and Jyh-Chian Chang¹

Department of Electrical and Electronic Engineering, Chung Cheng Institute of Technology,
National Defense University

Department of Information Communications, Kainan University

ABSTRACT

Additive Wavelet Transform (AWT) and Smoothing Filter-based Intensity Modulation (SFIM) can quickly merge massive volumes of data from new satellite imagery (such as IKONOS and QuickBird) without the problem of spectral mismatching. However, the amount of spatial details injected mainly relies on the designed low-pass filter. To tackle this problem, an adjustable AWT-SFIM approach is proposed in this work that only a half-size kernel is used to preserve spectral information and adjust spatial details. Experimental results demonstrate that the proposed technique can provide superior improvements than the original methods, that is, to maximize spatial details and minimize color distortion, simultaneously. In addition, the fused image often requires some further processes for image enhancement in many applications. The proposed approach is not only providing excellent performance on fusion, but also can sharpen image in the same time by simply tuning a weighting parameter k.

Keywords: Image fusion, additive wavelet transform, smoothing filter-based intensity modulation.

適用於 IKONOS/QuickBird 衛星影像融合之 可調整式加法性小波轉換及平滑濾波亮度調變影像融合法

杜德銘 程文雋 張劍平 張志堅1

國防大學理工學院電機電子工程研究所 1 開南大學資訊傳播系

摘 要

法性小波轉換(AWT)及平滑濾波亮度調變法(SFIM)均可在不產生頻譜失真問題的情況下,快速地融合大量的衛星影像資料(如 IKONOS 及 QuickBird 衛星影像)。然而,在此融合過程中,空間細節注入的多寡,端賴其低通濾波器設計的良劣。為了有效處理此問題,本研究提出了一個結合加法性小波轉換及平滑濾波亮度調變法之可調整式影像融方法,僅需使用原來一半大小的濾核,即可達到保留頻譜資訊及注入空間細節的目的。實驗結果證明,所提方法確可大幅改善原有技術,即達最大空間細節及最小色彩失真之目的。此外,在大部份的應用,融合後的影像通常需要再進行一些後處理。我們提出的方法,只需透過權重變數 k 的調整,不僅可提供絕佳的融合效果,亦可同時達到影像銳化的目地。

關鍵詞:影像融合、加法性小波轉換、平滑濾波亮度調變法

文稿收件日期 97.3.28.; 文稿修正後接受日期 97.10.30. Manuscript received March 28, 2008; revised October 30, 2008.

I. INTRODUCTION

Image fusion techniques aim at merging the information expressed by imagery acquired with different spatial and spectral resolution from satellites or aerial platforms. It has become a powerful tool in many remote sensing applications requiring both high spatial and spectral resolution, such as feature detection, change analysis, urban monitoring, land cover classification, and GIS-based applications.

In the remote sensing community. intensity-hue-saturation (IHS) and Brovey transform (BT) are two simplest image fusion methods that have been used as standard procedures in commercial packages, e.g. PCI Geomatics [1], RSI ENVI [2], and ERDAS IMAGINE [3]. Although the spatial resolution is normally improved, the color composite is distorted. This is turned into more apparent when the high-resolution satellites, **IKONOS** QuickBird images, become available, where they are marked with spectral disparities between multispectral (MS) bands and the panchromatic (Pan) band. To understand the influence of spectral response on the fusion of IKONOS/QuickBird images, the relative spectral responses depicted in Fig. 1 are investigated in detail. For comparison purpose, the Fig. 1(b), the spectral response of OuickBird imagery has been normalized. Ideally, the red (R), green (G), and blue (B) bands should fall just within the spectral range of the Pan band, e.g. the spectral response of Formosat-2 as shown in Fig. 2.

From Fig. 1, however, it appears that the green and blue bands overlap substantially, and the blue band mostly falls outside the 3-dB cutoff of the Pan band. Furthermore, the response of the Pan band is extended beyond the NIR band. Obviously, the color distortion problem in IHS/BT fusion results from such mismatches, in that Pan and intensity (I) are not spectrally similar. Recently, more attention has been paid on the spectral fidelity of image fusion methods [4-8]. In the mean time, we had introduced a saturation adjustable IHS-BT (SA-IHS-BT) fusion technique for IKONOS/QuickBird imagery [9] in our recent work, to balance the color distortion on saturation compression and stretching. However, even though the SA-IHS-BT approach can provide the best tradeoff between spectral and spatial details, it still can not reach the goal, that is, to maximize spatial details and minimize color distortion simultaneously.

In contrast with IHS and BT methods, Additive

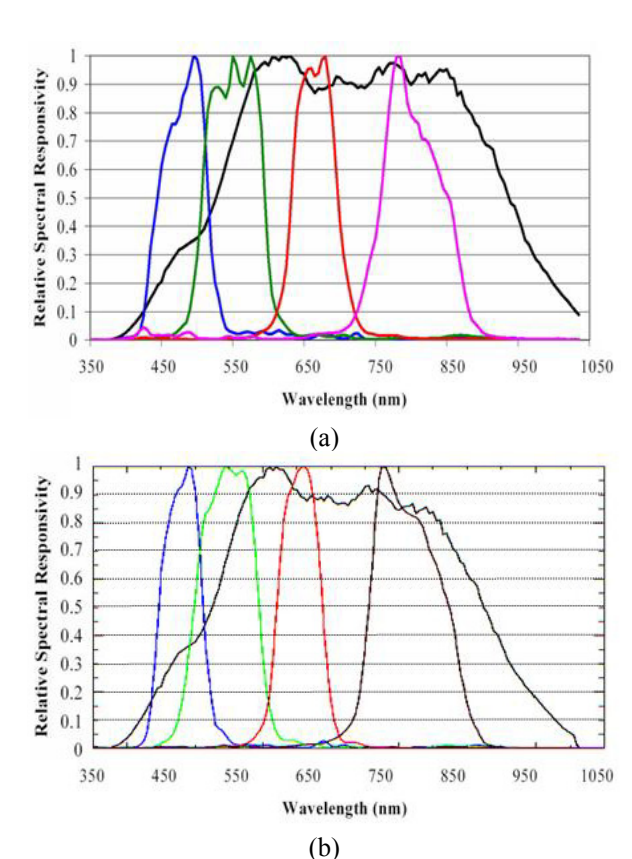


Fig. 1. The spectral responses of (a) IKONOS imagery and (b) QuickBird imagery.

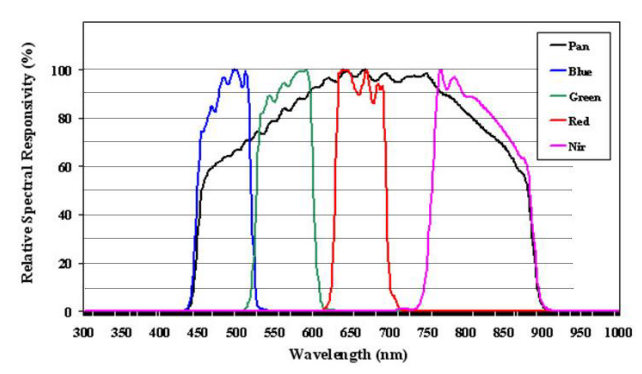


Fig. 2. The spectral responses of Formosat-2 imagery.

Wavelet Transform (AWT) [10] and Smoothing Filter-based Intensity Modulation (SFIM) [11] techniques inject the high-resolution spatial details only into each MS band, so they can cope with the spectral mismatching problem. That is, when compared to the color of the original MS image, the color of the fused image stays almost unchanged. In terms of spatial details, all spatial features of the Pan image are also perfectly integrated into the fused image. However, the success of injecting spatial

details mainly relies on the designed low-pass filter. For IKONOS/QuickBird image fusion, IKONOS and QuickBird provide individual spatial resolutions of MS imagery in 4 m and 2.4 m, and Pan imagery in 1 m and 0.6 m, respectively. Theoretically, the filter used should have a kernel size with the ratio between the spatial resolutions of the images. Liu [11] recommended that due to the sensitivity to co-registration, a filter slightly larger than the ratio would be appropriate. The ratio of Pan to MS equals four for IKONOS/QuickBird images. In the fusion phase, the MS image needs to be resized to the same size of Pan image, therefore, the ratio is 16. Then, the filter can be implemented by using a Gaussian low-pass filter with a 17x17 mask.

For IKONOS/QuickBird image fusion, however, the sizes of a standard scene are 11000x11000 pixels and 27000x28000 pixels, respectively. Therefore, the effort of applying a large filter on such huge images is computationally intensive. To tackle this problem, we have proposed a modified SFIM (MSFIM) approach recently [12], which can quickly merge a huge amount of different spatial resolution imagery with 5x5 filter. However, even though the MSFIM can greatly reduce the computation time of fusion, but it still has a little color distortion than original SFIM method. Therefore, we have tried another way to reduce the computation time, that is, to decompose the large kernel into small kernels and apply them sequentially. For doing so, we combine the AWT with SFIM methods and propose an adjustable AWT-SFIM approach that only a small 9x9 mask of Gaussian low-pass filter is required for IKONOS/QuickBird image fusion. Not only the computation time is reduced, the image resolution is also improved and the color is preserved as the original color composites, simultaneously. Also, the resultant image can be enhanced by tuning the weighting parameter k. To verify the efficacy of the proposed technique, experiments are carried out for evaluation on real images.

II. A NEW INSIGHT INTO AWT AND SFIM IMAGE FUSION

The wavelet-based image fusion of MS and PAN imagery becomes popular due to its ability to preserve the spectral fidelity of the MS imagery while improving its spatial quality. In which, the AWT method [10] directly injects the successive level

details of panchromatic image into the multispectral image. AWT can be represented by a fast IHS-like form given by

$$\begin{bmatrix} \mathbf{R}'_{\text{AWT}} \\ \mathbf{G}'_{\text{AWT}} \\ \mathbf{B}'_{\text{AWT}} \end{bmatrix} = \begin{bmatrix} \mathbf{R} \\ \mathbf{G} \\ \mathbf{B} \end{bmatrix} + \begin{bmatrix} \sum_{k=1}^{n} \mathbf{W}_{p_{k}} \\ \sum_{k=1}^{n} \mathbf{W}_{p_{k}} \\ \sum_{k=1}^{n} \mathbf{W}_{p_{k}} \end{bmatrix} = \begin{bmatrix} \mathbf{R} + \boldsymbol{\delta}_{\text{AWT}} \\ \mathbf{G} + \boldsymbol{\delta}_{\text{AWT}} \\ \mathbf{B} + \boldsymbol{\delta}_{\text{AWT}} \end{bmatrix}$$
(1)

which satisfies

$$Pan = \sum_{k=1}^{n} W_{pk} + \hat{P}an = \delta_{AWT} + \hat{P}an$$

and
$$\delta_{AWT} = \sum_{k=1}^{n} W_{Pk} = Pan - \hat{P}an$$

where $[R, G, B]^T$ is obtained from the up-sampled original MS image, \hat{P} an is the smooth version of Pan image, and δ_{AWT} denotes the multi-resolution wavelet plane.

Compared with the AWT method, the SFIM [11] approach is a ratio fusion technique that the fused image is produced by the product of the topography and texture of the higher resolution Pan image and the lower resolution MS image. It can be operated by a BT-like form represented by

$$\begin{bmatrix}
R'_{SFIM} \\
G'_{SFIM} \\
B'_{SFIM}
\end{bmatrix} = \frac{\text{Pan}}{\hat{P}\text{an}} \cdot \begin{bmatrix}
R \\
G \\
B
\end{bmatrix} = \gamma_{SFIM} \cdot \begin{bmatrix}
R \\
G \\
B
\end{bmatrix}$$
(2)

where $\gamma_{\text{SFIM}} = \text{Pan/Pan}$.

In contrast with the AWT and SFIM methods, IHS and BT can be operated by

$$\begin{bmatrix} R'_{IHS} \\ G'_{IHS} \\ B'_{IHS} \end{bmatrix} = \begin{bmatrix} R + (Pan - I) \\ G + (Pan - I) \\ B + (Pan - I) \end{bmatrix} = \begin{bmatrix} R + \delta_{IHS} \\ G + \delta_{IHS} \\ B + \delta_{IHS} \end{bmatrix}$$
and
$$\begin{bmatrix} R'_{BT} \\ G'_{BT} \\ B'_{BT} \end{bmatrix} = \frac{Pan}{I} \cdot \begin{bmatrix} R \\ G \\ B \end{bmatrix} = \gamma_{BT} \cdot \begin{bmatrix} R \\ G \\ B \end{bmatrix}$$
(3)

where $\delta_{\text{IHS}} = \text{Pan} - \text{I}$, I = (R + G + B)/3, and $\gamma_{\text{BT}} = \text{Pan/I}$. From the viewpoint of signal analysis,

 $\gamma_{\scriptscriptstyle \mathrm{BT}}$ and $\gamma_{\scriptscriptstyle \mathrm{SFIM}}$ are the multiplicative high frequency signals as the modulation factors while $\delta_{\scriptscriptstyle \mathrm{IHS}}$ and $\delta_{\scriptscriptstyle \mathrm{AWT}}$ are the additive high frequency signals as the injection factors for image fusion. Both of them can be treated as the spatial details of the Pan image.

However, the vegetation areas appear of relatively high reflectance in near infrared (NIR) and Pan bands, and low reflectance in RGB bands. Furthermore, because the effect of the NIR band is not included in I for the vegetation areas, the DN values in I are much smaller than those in Pan. This will result in the significant color distortion in green vegetation regions of the fused image by the IHS and BT methods. Fortunately, this distortion does not occur in the AWT and SFIM methods because they use Pan rather than I when injecting the spatial details to MS imagery. For IKONOS/QuickBird image fusion by using IHS/BT methods, it is thought that the relation of the pixel value of Pan and each band of MS (R, G, B and NIR) will be maintained by putting four parameters in (4) [13, 14]:

$$Pan \approx a \cdot R + b \cdot G + c \cdot B + d \cdot NIR = I$$
 (4)

To evaluate spatial and spectral changes generated by AWT and SFIM, (1) and (2) are substituted into the following two RGB-IHS conversion models. The first one is a linear transformation [14]:

$$\begin{bmatrix} I \\ vI \\ v2 \end{bmatrix} = \begin{bmatrix} 1/3 & 1/3 & 1/3 \\ -\sqrt{2}/6 & -\sqrt{2}/6 & 2\sqrt{2}/6 \\ 1/\sqrt{2} & -1/\sqrt{2} & 0 \end{bmatrix} = \begin{bmatrix} R \\ G \\ B \end{bmatrix}$$
and
$$\begin{bmatrix} R \\ G \\ B \end{bmatrix} = \begin{bmatrix} 1 & -1/\sqrt{2} & 1/\sqrt{2} \\ 1 & -1/\sqrt{2} & -1/\sqrt{2} \\ 1 & \sqrt{2} & 0 \end{bmatrix} \begin{bmatrix} I \\ vI \\ v2 \end{bmatrix}$$
 (5)

Hue (H) and saturation (S) are defined by the internal variables v1 and v2, and represented by

H =
$$\tan^{-1} \left(\frac{v^2}{v^1} \right)$$
 and S = $\sqrt{v l^2 + v^2}$ (6)

An alternative RGB-IHS conversion model is a nonlinear transformation. That is defined by

$$I = [R + G + B]/3$$
 (7-1)

$$H = \begin{cases} \cos^{-1}(\varphi), & \text{if } G \ge R \\ 2\pi - \cos^{-1}(\varphi), & \text{if } G \le R \end{cases}$$

$$\varphi = \frac{(2B - G - R)/2}{\sqrt{(B - G)^2 + (B - R)(G - R)}}$$
(7-2)

and
$$S = 1 - \frac{3\min(R, G, B)}{R + G + B} = \frac{I - a}{I}$$
,

where
$$a = \min(R, G, B)$$
 (7-3)

Originated from the previous comparisons between IHS and BT [9], we can draw the following conclusions. In practical applications, the IHS-like method works properly under the nonlinear RGB-IHS conversion system, while the BT-like method works in the linear RGB-IHS conversion system. Hence, for AWT method, by substituting (1) into (7), we can get

$$I'_{AWT} = (R'_{AWT} + G'_{AWT} + B'_{AWT})/3$$

$$= I + \delta_{AWT} = Pan_{AWT}$$
(8-1)

$$\frac{\varphi'_{AWT} = (2B'_{AWT} - G'_{AWT} - R'_{AWT})/2}{\sqrt{(B'_{AWT} - G'_{AWT})^2 + (B'_{AWT} - R'_{AWT})(G'_{AWT} - R'_{AWT})}}$$

$$= \varphi$$
(8-2)

$$S'_{AWT} = 1 - \frac{3\min(R'_{AWT}, G'_{AWT}, B'_{AWT})}{R'_{AWT} + G'_{AWT} + B'_{AWT}}$$

$$= \frac{I - a}{Pan_{AWT}} = \frac{I}{I + (Pan - \hat{P}an)} \cdot S$$
(8-3)

where $Pan_{AWT} = I + \delta_{AWT} = I + (Pan - \hat{P}an)$. This is the intensity component of the fused image. Meanwhile, for SFIM method, by substituting (2) into (5), we have

$$\begin{bmatrix} \mathbf{R}'_{\text{SFIM}} \\ \mathbf{G}'_{\text{SFIM}} \end{bmatrix} = \gamma_{\text{SFIM}} \cdot \begin{bmatrix} \mathbf{R} \\ \mathbf{G} \\ \mathbf{B} \end{bmatrix} = \frac{\text{Pan}}{\hat{\mathbf{P}} \text{an}} \cdot \begin{bmatrix} 1 & -1/\sqrt{2} & 1/\sqrt{2} \\ 1 & -1/\sqrt{2} & -1/\sqrt{2} \\ 1 & \sqrt{2} & 0 \end{bmatrix} \begin{bmatrix} \mathbf{I} \\ \mathbf{v} \mathbf{l} \\ \mathbf{l} \\ \mathbf{v} \mathbf{l} \end{bmatrix}$$

$$= \begin{bmatrix} \text{Pan}_{\text{SFIM}} \\ \text{Pan}_{\text{SFIM}} \\ \text{Pan}_{\text{SFIM}} \end{bmatrix} + \begin{bmatrix} -1/\sqrt{2} & 1/\sqrt{2} \\ -1/\sqrt{2} & -1/\sqrt{2} \\ \sqrt{2} & 0 \end{bmatrix} \begin{bmatrix} \gamma_{\text{SFIM}} \cdot \mathbf{v} \mathbf{l} \\ \gamma_{\text{SFIM}} \cdot \mathbf{v} \mathbf{l} \end{bmatrix}$$

$$\begin{bmatrix} \gamma_{\text{SFIM}} \cdot \mathbf{v} \mathbf{l} \\ \gamma_{\text{SFIM}} \cdot \mathbf{v} \mathbf{l} \end{bmatrix}$$

$$\begin{bmatrix} \gamma_{\text{SFIM}} \cdot \mathbf{v} \mathbf{l} \\ \gamma_{\text{SFIM}} \cdot \mathbf{v} \mathbf{l} \end{bmatrix}$$

$$\begin{bmatrix} \gamma_{\text{SFIM}} \cdot \mathbf{v} \mathbf{l} \\ \gamma_{\text{SFIM}} \cdot \mathbf{v} \mathbf{l} \end{bmatrix}$$

where $\operatorname{Pan}_{\text{SFIM}} = \gamma_{\text{SFIM}} \cdot I = (\operatorname{Pan/\widehat{P}an}) \cdot I$. This is also the intensity component of fused image. The hue and saturation components can be calculated by

$$H'_{SFIM} = \tan^{-1} \left(\frac{\gamma_{SFIM} \cdot \nu^{2}}{\gamma_{SFIM} \cdot \nu^{1}} \right) = H \quad \text{and}$$

$$S'_{SFIM} = \gamma_{SFIM} \cdot \sqrt{\nu^{2} + \nu^{2}} = \frac{Pan}{\hat{P}an} \cdot S$$
(10)

By observing (8), (9) and (10), it can be noted that AWT and SFIM methods keep the same hue value as its corresponding value of the original RGB image, but the saturation value has been altered. Due to the fact that both spatial details and spectral distortion of AWT and SFIM mainly rely on the designed low-pass filter of Pan, the color distortion can be eliminated by applying a smaller smooth-filter mask to Pan and forcing $\delta_{\mbox{\tiny AWT}}$ and $\gamma_{\mbox{\tiny SFIM}}$ values to be close to zero and one, respectively. After doing so, however, the spatial resolution of the fused image becomes worse than that of Pan. To avoid losing the spatial resolution of the fused image, a large smooth-filter mask should be selected for those two methods to increase spatial details. Therefore, interfering between these two factors, to design an appropriate and optimal filter becomes nontrivial. After comparing (8-3) and (10), we also found that the color distortion produced by AWT is inversely proportional to that generated by SFIM method. That is, if Pan value is less then the Pan value, the saturation value is expanded or stretched $(S'_{AWT} > S)$ by AWT method while the saturation value is compressed $(S'_{SFIM} < S)$ by SFIM method. Similar conclusions have been drawn in our previous work [9].

Preliminary studies have shown that the quality of the fused imagery produced by the AWT technique is a function of the number of decomposition levels. If fewer decomposition levels are applied, the spatial quality of the fused images is less satisfactory. However, if excessive levels are applied, the spectral similarity between the original MS and the fused imagery decreases. On the contrary, SFIM only uses a large filter to produce Pan image without considering the number of decomposition levels. According to [15], the filter used should have a kernel size slightly larger than the ratio between the spatial and spectral resolutions of the images. That is, when AWT or SFIM is used for fusing IKONOS/QuickBird imagery, a 17x17 mask of Gaussian low-pass filter is required to produce the Pan image. In practice, however, IKONOS and QuickBird imagery are huge; they may have tens of thousands of rows and columns in each band. Thus, a large filter consumes more computational power and takes a longer waiting time to generate the results. Therefore, the filter design is the key issue we need to consider for fusing images by AWT or SFIM methods.

III. AN INTEGRATED AWT-SFIM IMAGE FUSION APPROACH

To cope with the problem stated above, large kernels can be decomposed into small kernels for sequential applications. Thus, we propose to combine AWT and SFIM into an integrated approach and only use a smaller mask to produce \hat{P} an. The integrated approach can be represented by

$$\begin{bmatrix} R'_{AWT-SFIM} \\ G'_{AWT-SFIM} \\ B'_{AWT-SFIM} \end{bmatrix} = \begin{bmatrix} R'_{SFIM,s} \\ G'_{SFIM,s} \\ B'_{SFIM,s} \end{bmatrix} + k \cdot \begin{bmatrix} \delta_{AWT,s} \\ \delta_{AWT,s} \\ \delta_{AWT,s} \end{bmatrix}$$

$$= \frac{Pan}{\hat{P}an_{s}} \cdot \begin{bmatrix} R \\ G \\ B \end{bmatrix} + k \cdot \begin{bmatrix} Pan - \hat{P}an_{s} \\ Pan - \hat{P}an_{s} \\ Pan - \hat{P}an_{s} \end{bmatrix}$$
(11)

where $\left[R'_{AWT-SFIM}, G'_{AWT-SFIM}, B'_{AWT-SFIM}\right]^T$ the produced fused image, the internal fused image $\left[R'_{SFIM,s}, G'_{SFIM,s}, B'_{SFIM,s}\right]^T$ is obtained from the resized original image $[R, G, B]^T$ simply by intensity modulation, and Pan is a slight smoothed version of Pan image compared with Pan. Obviously, the distortion of the internal $[R'_{SFIM,s}, G'_{SFIM,s}, B'_{SFIM,s}]^T$ is less than that produced by the original SFIM method since the filter size used here is smaller than that by of SFIM. However, we might encounter the sequence that not enough details are shown in the spatial information. This is due to that Pan is more similar to Pan than Pan produced by a 17x17 filter. To embed enough spatial details, a AWT-like approach in (11) is used to inject additional spatial information by $\delta_{\text{\tiny AWT,s}} = \text{Pan} - \hat{\text{P}an}_{\text{\tiny s}}$. The weighting parameter k controls the degree of additional spatial details added into the fused image. Since we combine both injection methods of AWT and SFIM, ideally, we can use only a half size of kernel to generate the pan image. In this work, a

9x9 mask of Gaussian low-pass filter is used in (11).

As described in the previous section, SFIM technique and AWT method suffer from saturation compression and saturation stretch on same regions, respectively. Furthermore, the saturation distortion problem can be reduced by the proposed approach to fuse images because the color distortion in the internal fused image $\left[R'_{\text{SFIM,s}}, G'_{\text{SFIM,s}}, B'_{\text{SFIM,s}}\right]^T$ will be mitigated by applying the AWT method.

Due to the landscape variation changes for different scenes, the weighting parameter k cannot be theoretically modeled and determined. In this work, the lower bound of k is determined by the intensity component of fused image. By referring to (11), the intensity component is given by

$$I'_{AWT-SFIM} = \frac{Pan}{\hat{P}an_s} \cdot I + k \cdot (Pan - \hat{P}an_s)$$
 (12)

Due to the ratio of Pan to $\hat{P}an_s$ equals 9 and the ratio of Pan to I equals 16, when k=0.5, the value of $I'_{AWT-SFIM}$ is close to Pan. Hence, if Pan is set to one, we get

$$I'_{AWT-SFIM} = \frac{Pan}{\hat{P}an_s} \cdot I + k \cdot (Pan - \hat{P}an_s)$$

$$= \frac{1}{1/9} \cdot (1/16) + 0.5 \cdot (1 - (1/9)) \approx 1 = Pan.$$

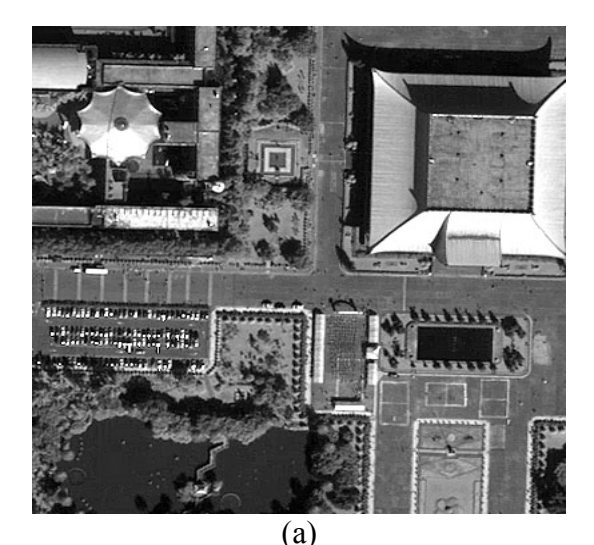
This formula can also verify that the kernel size of AWT and SFIM should be 17x17. That is,

$$\begin{split} &I'_{_{AWT}} = I + (Pan - \hat{P}an) \\ &= (1/16) + (1 - (1/17)) \cong 1 = Pan \\ ∧ \quad I'_{_{SFIM}} = \frac{Pan}{\hat{P}an} \cdot I = \frac{1}{1/17} \cdot (1/16) \cong 1 = Pan \;. \end{split}$$

To further validate the above formulas, 153 IKONOS and 46 QuickBird images, covering different areas, are used in our experiments. When k = 0.5, the fused image produced by (11) is demonstrated to be very similar to the spatial and spectral results achieved by AWT and SFIM. On the other hand, when k > 1, a sharpened image is generated by (11) and it contains more spatial details than those produced by either AWT or SFIM, just like the fused image has done the sharpness enhancement. A recommendatory range for k is $0.5 \le k \le 1.5$. To verify the efficacy of the proposed techniques, real images are used in the experiments in the next section.

IV. EXPERIMENTAL RESULTS

Since the spatial resolution of the QuickBird images is better than that of the IKONOS ones, it is easier to check the changes of spatial details and spectral information by using QuickBird images. The data used for the experiment is an image scene on Taipei, Taiwan, taken by the QuickBird satellite sensor in June 2004. The size of image is 10000×10000 pixels. For the purpose of clear visualization, we only display small chips in all results. The Pan image and the corresponding resized RGB images of the test data are displayed in Fig. 3(a) and 3(b), respectively. AWT, SFIM and the proposed fusion method specified in (1), (2), and (11), respectively, are tested individually.



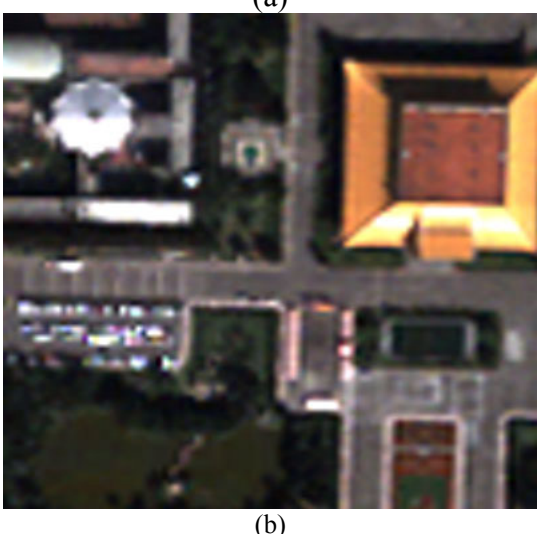


Fig. 3. A subsection of Taipei, Taiwan (a) The original Pan image. (b) The corresponding RGB image.

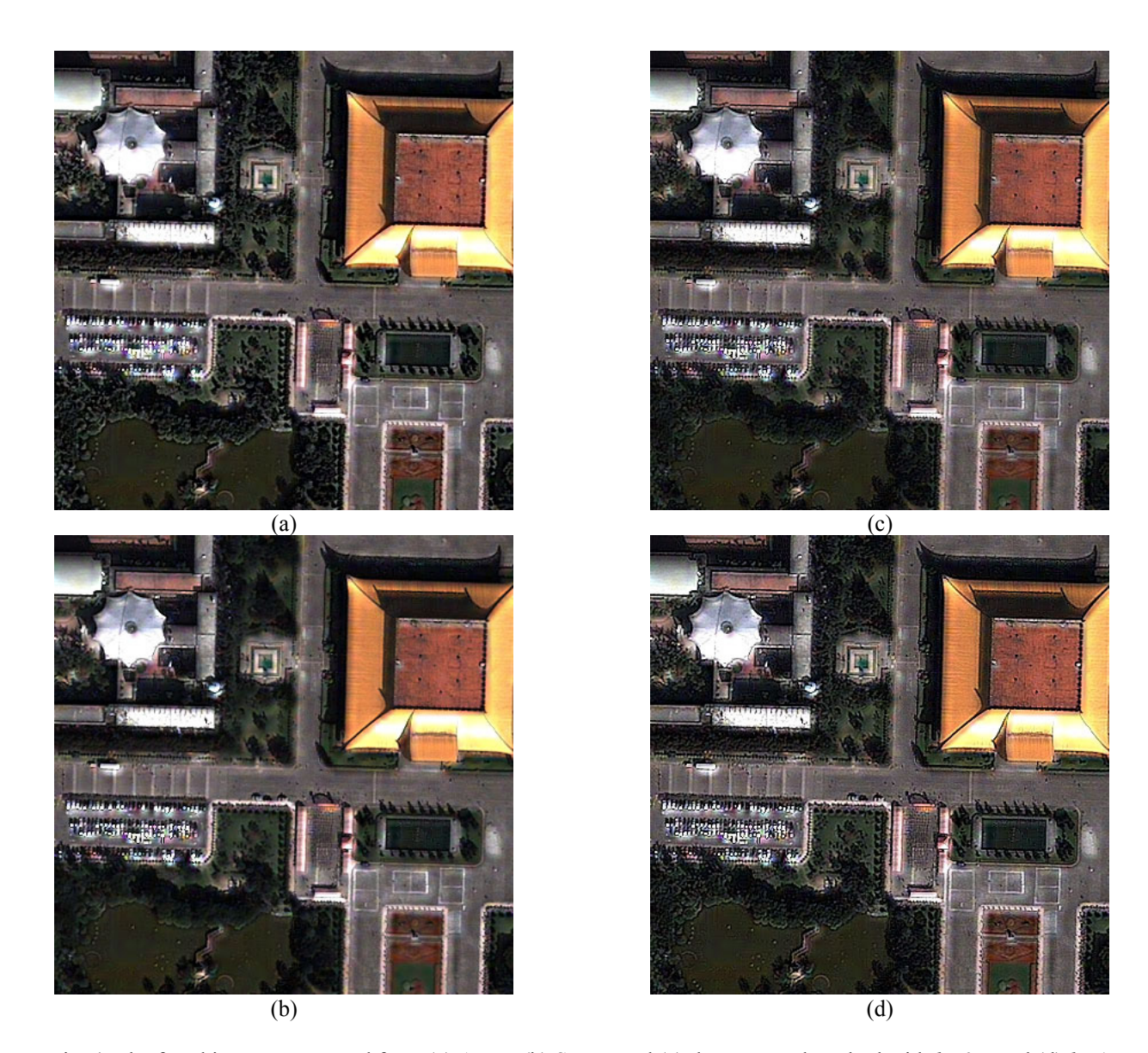


Fig. 4. The fused images generated from (a) AWT, (b) SFIM, and (c) the proposed method with k = 0.5 and (d) k = 1.

The fusion results achieved by AWT and SFIM fusion methods are displayed in Fig. 4(a) and 4(b). Fig. 4(c) and 4(d) show the fused images produced by the proposed method by setting k = 0.5 and 1, respectively. It can be easily observed that, except the green vegetation regions, the fused images generated by the three fusion methods well demonstrate that all colors are almost unchanged. In terms of spatial details, all spatial features of the Pan image are also perfectly injected into the fused images.

By visually inspecting the green vegetation regions, we can find that SFIM (Fig. 4(b)) has preserved the best spectral information, while AWT

(Fig. 4(a)) has provided the most spatial details. The results obtained from the proposed fusion method with k = 0.5 (Fig. 4(c)) are similar to that from SFIM, while the results with k = 1 (Fig. 4(d)) are close to that from AWT.

Band-to-band correlation coefficients (CCs) between the re-sampled original and the fused bands are displayed for all those three image fusion methods in Table 1. The correlation coefficients of those metrics are consistent with the results produced by visual evaluations. After using a larger set of IKONOS and QuickBird images, further experiments have also reached similar conclusions.

In summary, the proposed method in this study offers a feasible solution for merging massive volumes of IKONOS/QuickBird image data. Experimentally, the computation time using a mask of 9x9 is three times faster than using a mask of 17x17. For better visualization and printing quality of thefused image from the AWT and SFIM methods, this can be achieved by using an un-sharp mask filter after the fusion process.

However, with the proposed method, we can reach same performance only by increasing the k value. As an illustrated example, Fig. 5(a) shows the fused image produced by AWT fusion followed by the processing of an un-sharp mask (with Amount: 100%, Radius: 1 pixel, and Threshold: 0 levels in Photoshop).

Table 1. Correlation coefficients associated with the three fused images in Fig. 4.

	AWT	SFIM	AWT-SFIM $(k = 0.5)$	AWT-SFIM $(k = 1)$			
	The intensity component of fused image $I = (R+G+B)/3$						
Pan	0.838	0.814	0.809	0.836			
Pan	0.850	0.822	0.816	0.842			
Pan	0.782	0.747	0.741	0.771			
MS		The	fused image; Re	GB			
R	0.950	0.947	0.957	0.951			
G	0.938	0.938	0.949	0.942			
В	0.936	0.935	0.947	0.939			

Fig. 5(b) demonstrates the fused image by the proposed method with k = 1.5. The correlation coefficient between those two images is 0.99. However, Fig. 5(b) has better visual effect than Fig. 5(a). In addition, Ferzli et al. [16] proposed a noise immune wavelet based sharpness (NIWBS) metric method which can be adopted as one index for sharpness evaluation. That is, the sharper the image, the lower value the metric is. For example, Fig. 6 demonstrates that the sharpness is defined by the boundaries between zones of different gray levels. It is illustrated by the bar patterns with increasing spatial frequencies. Although Fig. 6(b) is added with pepper and salt noise by the density 0.01, the obtained NIWBS values of Fig. 6(a) and 6(b) are 4.43 and 4.67, respectively. This indicates correctly that the image in Fig 6(a) has almost the same sharpness as the one in Fig. 6(b). Furthermore, the NIWBS values of Fig. 6(c) and 6(d) are 5.57 and 6.03, respectively. From the NIWBS values of Fig. 6(b) and 6(c), it shows that the sharper image can be better distinguished from noisy images. Thus, the NIWBS is an effective sharpness evaluation index.

The NIWBS metric of demonstrated images are shown in Table 2. The fused image with higher weighting parameter k has better sharpness result. Moreover, the Fig. 5(b) is not only has better visual effect than Fig. 5(a), but also has better sharpness index too.

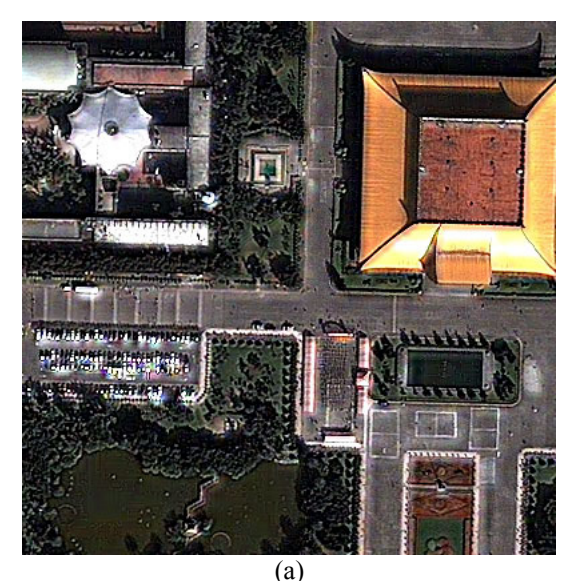




Fig. 5. The fused images generated from (a) AWT followed by the processing of an un-sharp mask filter and (b) the proposed method with k = 1.5

	AWT	SFIM	AWT-SFIM $(k = 0.5)$	AWT-SFIM $(k = 1)$	AWT & un-sharp mask filter	AWT-SFIM $(k = 1.5)$
Fig. #	4 (a)	4 (b)	4 (c)	4 (d)	5 (a)	5 (b)
NIWBS	4.07	4.31	4.03	3.97	4.01	3.94
					ACKNOWI FDO	~FMFNT(

Table 2. Sharpness index (NIWBS) associated with the all fused images in Fig. 4 and 5.

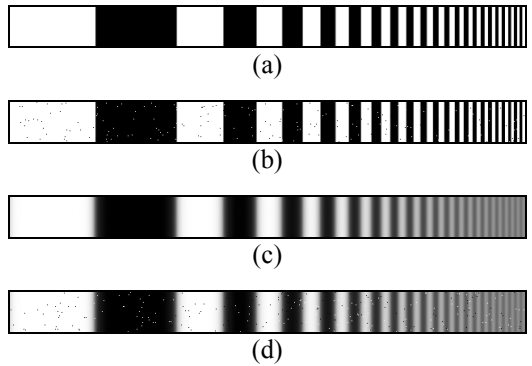


Fig. 6. Bar patterns with increasing spatial frequencies [17]. (a) Sharp pattern with NIWBS=4.43, (b) Sharp pattern added with pepper and salt noise by the density of 0.01, NIWBS=4.67, (c) Blurred pattern with NIWBS=5.75, (d) Blur pattern added with pepper and salt noise by the density of 0.01, NIWBS=6.03.

V. CONCLUSIONS

The wavelet-based fusion scheme, AWT methods, has become popular due to its ability to preserve the spectral fidelity of the MS imagery while improving its spatial quality. This is practically important if the fused imagery is used for the application of automatic classification. For image fusion, spatial enhancement, spectral preservation and computation speed are all critical issues. In this work, the proposed algorithm is developed from the idea that combining AWT with SFIM could provide lower computation time and better information adjustment ability. In addition, the proposed approach can perform the image enhancement and fusion simultaneoursly as well. By comparing to SFIM and AWT methods in the experimental results, the proposed method can achieve better performance than those two methods in preserving both spectral and spatial information in the fusion process. Since the proposed approach has no spectral mismatching problem, the algorithm is not only feasible for the fusion of IKONOS/QuickBird imagery but also for merging multi-source remote sensing images.

ACKNOWLEDGEMENTS

The authors would like to thank RITI Technology, Inc., for providing Quickbird imagery. RITI is an agent in Taiwan of DigitalGlobe Company. Also thank the National Science Council of the Republic of China for financially supporting this work under Contract No. NSC 94-2213-E-014-013.

REFERENCES

- [1] PCI Geomatics Enterprises Inc., Geomaticas 10.0 User Manual, PCI Geomatics Enterprises Inc. Canadian, 2006.
- [2] Research Systems Inc., ENVI 4.3 User's Guide, Research Systems Inc. USA, 2006.
- [3] Leica Geosystems GIS & Mapping Inc., ERDASIMAGINE 8.9 User's Guide, Leica Geosystems GIS & Mapping Inc. USA, 2006.
- [4] González-Audícana, M., Otazu, X., Fors, O., and Alvarez-Mozos, J., "A low computational-cost method to fuse IKONOS images using the spectral response function of its sensors," IEEE Transactions on Geoscience and Remote Sensing, Vol. 44, No. 6, pp. 1683-1691, 2006.
- [5] Aiazzi, B., Alparone, L., Baronti, S., Garzelli, A., and Selva, M., "MTF-tailored multiscale fusion of high-resolution MS and Pan imagery," Photogrammetric Engineering and Remote Sensing, Vol. 72, No. 5, pp. 591-596, 2006.
- [6] Švab, A., and Oštir, K., "High-resolution image fusion: methods to preserve spectral and spatial resolution," Photogrammetric Engineering and Remote Sensing, Vol. 72, No. 5, pp. 565-572, 2006.
- [7] Zhang, Y., "Understanding image fusion," Photogrammetric Engineering and Remote Sensing, Vol. 70, No. 6, pp. 657-661, 2004.
- [8] Tu, T. M., Huang, P. S., Hung, C. L., and Chang, C. P., "A fast intensity-hue-saturation fusion technique with spectral adjustment for IKONOS imagery," IEEE Transactions on Geoscience and Remote Sensing Letters, Vol. 1, No. 4, pp.

- 309-312, 2004.
- [9] Tu, T. M., Lee, Y. C., Chang, C. P., and Huang, P. S., "Adjustable intensity-hue-saturation and Brovey transform fusion technique for IKONOS/ QuickBird imagery," Optical Engineering, Vol. 44, No. 11, pp. 116201.1-116201.10, 2005.
- [10] Núnez, J., Otazu, X., Fors, O., Prades, A., Pala, V., and Arbiol, R., "Multiresolution-based image fusion with additive wavelet decomposition," IEEE Transactions on Geoscience and Remote Sensing, Vol. 37, No. 3, pp. 1204-1211, 1999.
- [11] Liu, J. G., "Smoothing filter-based intensity modulation: a spectral preserve image fusion technique for improving spatial details," International Journal of Remote Sensing, Vol. 21, No. 18, pp. 3461-3472, 2000.
- [12] Tu, T. M., Lee, Y. C., Chang, C. P., and Huang, P. S., "Modified smoothing-filter-based technique for IKONOS-QuickBird image fusion," Optical Engineering, Vol. 45, No. 6, pp. 066201.1-066201.10, 2006.
- [13] Kalpoma K. A., and Kudoh J. I., "Image Fusion Processing for IKONOS 1-m Color Imagery," IEEE Transactions on Geoscience and Remote Sensing, Vol. 45, No. 10, pp. 3075-3086, 2007.
- [14] Aiazzi B., and Baronti S., "Improving Component Substitution Pansharpening Through Multivariate Regression of MS + Pan Data," IEEE Transactions on Geoscience and Remote Sensing, Vol. 45, No. 10, pp. 3230-3239, 2007
- [15] Ledley, R. S., Buas, M., and Golab, T. J., "Fundamentals of true-color image processing," IEEE Proceedings, 10th International Conference, Pattern Recognition Vol. 1, pp. 791-795, 1990.
- [16] Ferzli, R., and Karam, L. J., "No-Reference Objective Wavelet Based Noise Immune Image Sharpness Metric," in Proc. of the 2005 Int. Conf. on Image Processing (ICIP 2005), Genoa, pp. 405-408, 2005.
- [17] IMATEST LLC, Imatest-sharpness. http://www.imatest.com/docs/sharpness.html